

# A Quantitative Structural Investigation of the 0.1 wt % Nb–SrTiO<sub>3</sub>(001)/H<sub>2</sub>O Interface

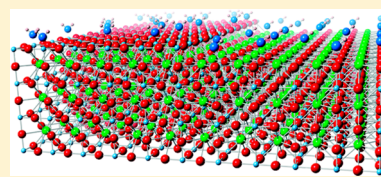
H. Hussain,<sup>†,‡,§</sup> X. Torrelles,<sup>§</sup> P. Rajput,<sup>‡,||</sup> M. Nicotra,<sup>†,¶</sup> G. Thornton,<sup>\*,†</sup> and J. Zegenhagen<sup>‡,△</sup>

<sup>†</sup>London Centre for Nanotechnology and Department of Chemistry, University College London, 20 Gordon Street, London WC1H OAJ, United Kingdom

<sup>‡</sup>ESRF, 6 rue Jules Horowitz, F-38000 Grenoble cedex, France

<sup>§</sup>Institut de Ciència de Materials de Barcelona (CSIC), Campus UAB, 08193 Bellaterra, Spain

**ABSTRACT:** Surface X-ray diffraction has been employed to elucidate the structure of the interface between a well-characterized (001) surface of 0.1 wt % Nb–SrTiO<sub>3</sub> and liquid H<sub>2</sub>O. Results are reported for the clean surface, the surface in contact with a drop of liquid water, and the surface after the water droplet has been removed with a flow of nitrogen. The investigation revealed that the clean surface, prepared via annealing in  $1 \times 10^{-2}$  mbar O<sub>2</sub> partial pressure, is unreconstructed and rough on a short length scale. The surface is covered with large terraces, the topmost layer of which is either TiO<sub>2</sub> or SrO with an area ratio of about 7/3. For the surface in contact with water, our results reveal that associative H<sub>2</sub>O adsorption is favored for the TiO<sub>2</sub>-terminated terrace whereas adsorption is dissociative for the SrO-terminated terrace, which validates recent first-principles calculations. After removal of the water droplet, the surface largely resembles the water-covered surface but now with a disordered overlayer of water present on the surface.



## INTRODUCTION

SrTiO<sub>3</sub> (STO) has received much attention over the years because of its importance in many applications such as photocatalysis,<sup>1</sup> as a gas sensor,<sup>2</sup> and as an anode for solid oxide fuel cells.<sup>3</sup> Water is arguably the most important adsorbate to investigate, since in many applications of STO it is either purposely or inadvertently exposed to the surface. Even in controlled conditions (such as ultrahigh vacuum (UHV)) water is usually one of the most abundant constituents in the residual, and so a great deal of importance is placed on understanding its interactions with the STO(001) surface. For this reason it has been the subject of a number of investigations.<sup>4–6</sup>

STO crystallizes in the cubic perovskite structure that is made up of alternating layers of TiO<sub>2</sub> and SrO, as shown in Figure 1. Depending on the preparation procedure, a mixed terminated or a singly terminated surface can be achieved for the (001) orientation producing a plethora of different phases and nanostructures.<sup>7–13</sup> The general consensus in the literature, with regards to the (1 × 1) phase, is that water dissociates on the SrO termination whereas molecular adsorption is preferred on the TiO<sub>2</sub> termination. A study by Iwahori et al.<sup>14</sup> using friction force microscopy was able to image the mixed terminated surface before and after exposure to several different partial pressures of water. They concluded that changes in the friction force were only visible for the SrO-terminated surface, being due to surface hydroxylation.

Several theoretical investigations have provided further evidence for the different adsorption modes seen in experimental work. A density functional theory (DFT) study by Baniecki et al.<sup>15</sup> found that the most favorable adsorbate configuration for the (1 × 1) SrO-terminated surface is a

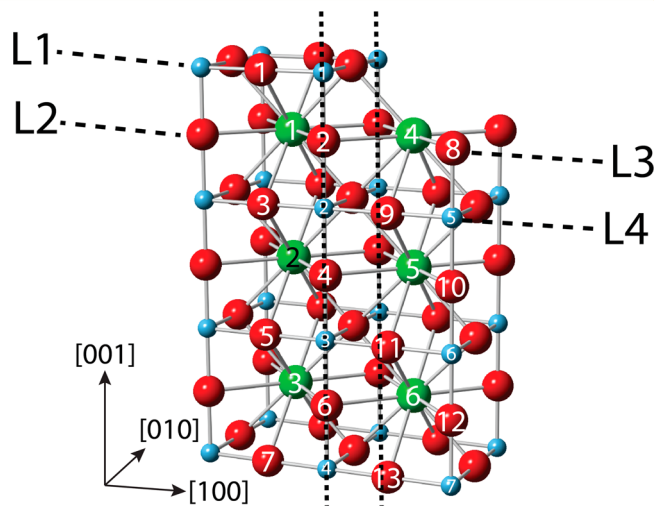


**Figure 1.** Ball-and-stick model representation of the SrTiO<sub>3</sub>(001) surface with the two terminations, TiO<sub>2</sub> and SrO, found in this study. Small light blue, large red, and largest green spheres are titanium, oxygen, and strontium atoms, respectively. The labeled layers (L1, L2, L3, and L4) are the same as used in Table 1. The numbering of the Ti, Sr, and O atoms is the same as used in Tables 2 and 3. Discontinuous lines indicate that the two surface unit cells correspond to the two different incoherent T1 and T2 terraces.

partially dissociated structure, whereas molecular adsorption was favored on the TiO<sub>2</sub>-terminated surface. These findings have been corroborated by other publications.<sup>16,17</sup> Much of our

Received: April 7, 2014

Published: April 23, 2014

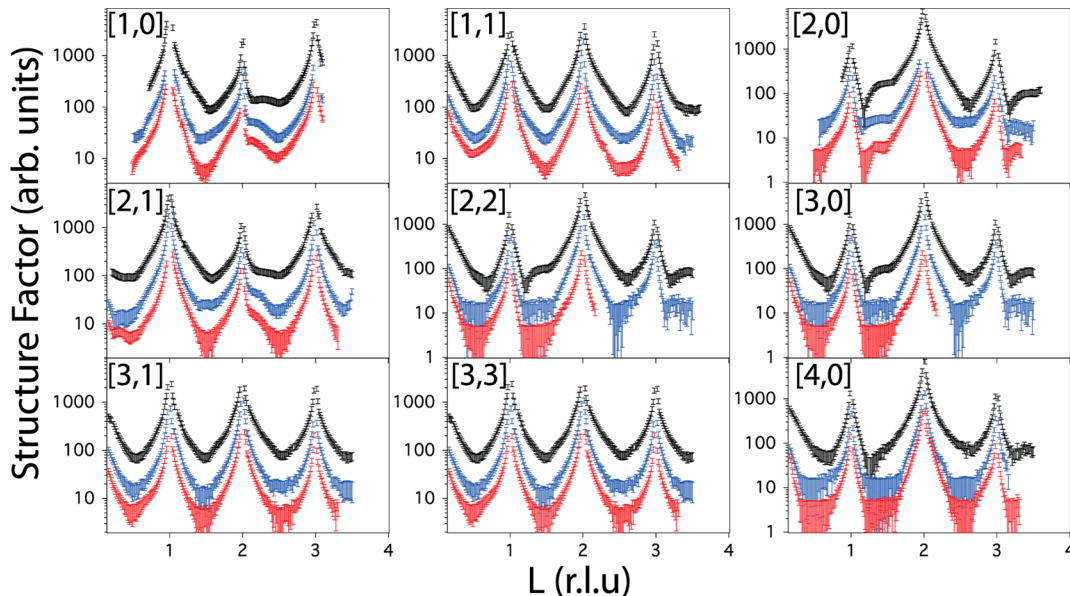


**Figure 2.** Comparison of experimental structure factors for the different conditions measured: clean (UHV), water-adsorbed, and nitrogen flow-dried surface are black (top), blue (middle), and red (bottom) error bars, respectively. Profiles are offset for clarity.

understanding of the interaction of water with STO is at monolayer or submonolayer coverage, and as far as we are aware there have been no quantitative experimental investigations of the structure at the STO(001) interface with liquid water. Here we provide a quantitative structural analysis of the STO(001)/liquid H<sub>2</sub>O interface using surface X-ray diffraction (SXRD).

## ■ EXPERIMENTAL SECTION

The experiments were carried out at the ID32 beamline of the European Synchrotron Radiation Facility (ESRF).<sup>18</sup> The X-ray measurements were performed with the samples at room temperature using a monochromatic focused beam with an energy of 17.7 keV ( $\lambda = 0.7 \text{ \AA}$ ), defined by slits to a size of (200  $\mu\text{m} \times 20 \mu\text{m}$ ). The surface (7 mm  $\times$  5 mm) of the 2 mm thick STO(001) sample (0.1 wt % Nb, Crystal GmbH, Berlin) underwent ultrasonic cleaning in acetone after which it was rinsed with deionized water. It was mounted to a Mo backplate via spot welding with Ta clips and inserted into the UHV chamber (base pressure of  $10^{-10} \text{ mbar}$ ). In order to produce a well-ordered clean surface, repeated cycles of annealing up to 700 °C in an O<sub>2</sub> partial pressure of  $1 \times 10^{-2} \text{ mbar}$  were performed until a sharp (1  $\times$  1) low-energy electron diffraction (LEED) pattern was obtained. Auger electron spectroscopy showed no signs of contamination within the detection limits.

STM measurements were made on the as-prepared surface. The images show that steps of less than unit cell height were present, consistent with earlier work<sup>19</sup> as well as with a mixed terminated surface.<sup>5,14,20</sup> After preparation, the sample was transferred to a small, portable, ion-pumped UHV chamber (“baby chamber”) with a base pressure in the  $10^{-9} \text{ mbar}$  range. It features a cylindrical shaped beryllium window, which allows unrestricted transmission of the incident and reflected X-ray beams.<sup>21</sup> It was taken to the experimental hutch and directly mounted on the six-circle diffractometer for the surface X-ray diffraction measurements. The STO(001) cubic surface unit cell was described by the lattice vectors ( $\mathbf{a}$ ,  $\mathbf{b}$ ,  $\mathbf{c}$ ) parallel to the [100], [010], and [001] directions, respectively, where  $a$  and  $b$

lie in the surface plane and  $c$  is perpendicular to the surface ( $a = b = c = 3.905 \text{ \AA}$ ).

The angle of incidence of the X-ray beam with respect to the surface was kept constant at 0.3° for all measurements with 2  $\times$  2 mm<sup>2</sup> slits in front of the detector, at 1 m from the beamspot on the sample. The surface terrace length was of the order of 0.65  $\mu\text{m}$ , calculated from the experimental estimation of the surface miscut angle (0.035°) obtained from the deviations of the experimental surface normal vector respect to the ideal one, i.e., (0,0,1). The experimental data were collected by measuring the scattered intensities at the desired momentum transfer  $q$  while rotating the surface around its normal, otherwise known as rocking scans. These data were then integrated and corrected in order to evaluate the structure factors of the different ( $h, k, l$ ) reflections, which when represented versus perpendicular momentum transfer are known as crystal truncation rods (CTRs).<sup>22</sup> The overall stability of the system was controlled by monitoring the intensity evolution of the highly sensitive (1, 0, 0.5) surface reference reflection at regular intervals of time to monitor sample degradation and/or evolution. No significant changes were observed throughout the duration of the experiment. From the angular width of this reflection ( $\Delta\theta_{\text{fwhm}} = 0.0008 \text{ r.l.u.}$ ) the surface terrace size is about 0.5  $\mu\text{m}$ , close to the value expected from the surface miscut angle.

A large data set of 20 CTRs for the as-prepared surface was measured. Immediately after, the baby chamber was vented with and kept in a constant flow of nitrogen to reduce surface contamination while an electrochemical droplet cell for controlled water exposure was installed. The ultrapure water used was subjected to several freeze pump thaw cycles to ensure a contaminant free liquid. With the use of a computer-controlled pumping system and endoscope, a droplet of approximately 4 mm in diameter was brought into contact with the sample surface creating a meniscus.<sup>21</sup> A further 13 CTRs were measured in these conditions. To determine any possible residual effects on the surface due to the adsorption of water, 10 CTRs were measured after removal of the water droplet by “drying” with a flow of nitrogen. A comparison of the experimental structure factors is shown in Figure 2. The

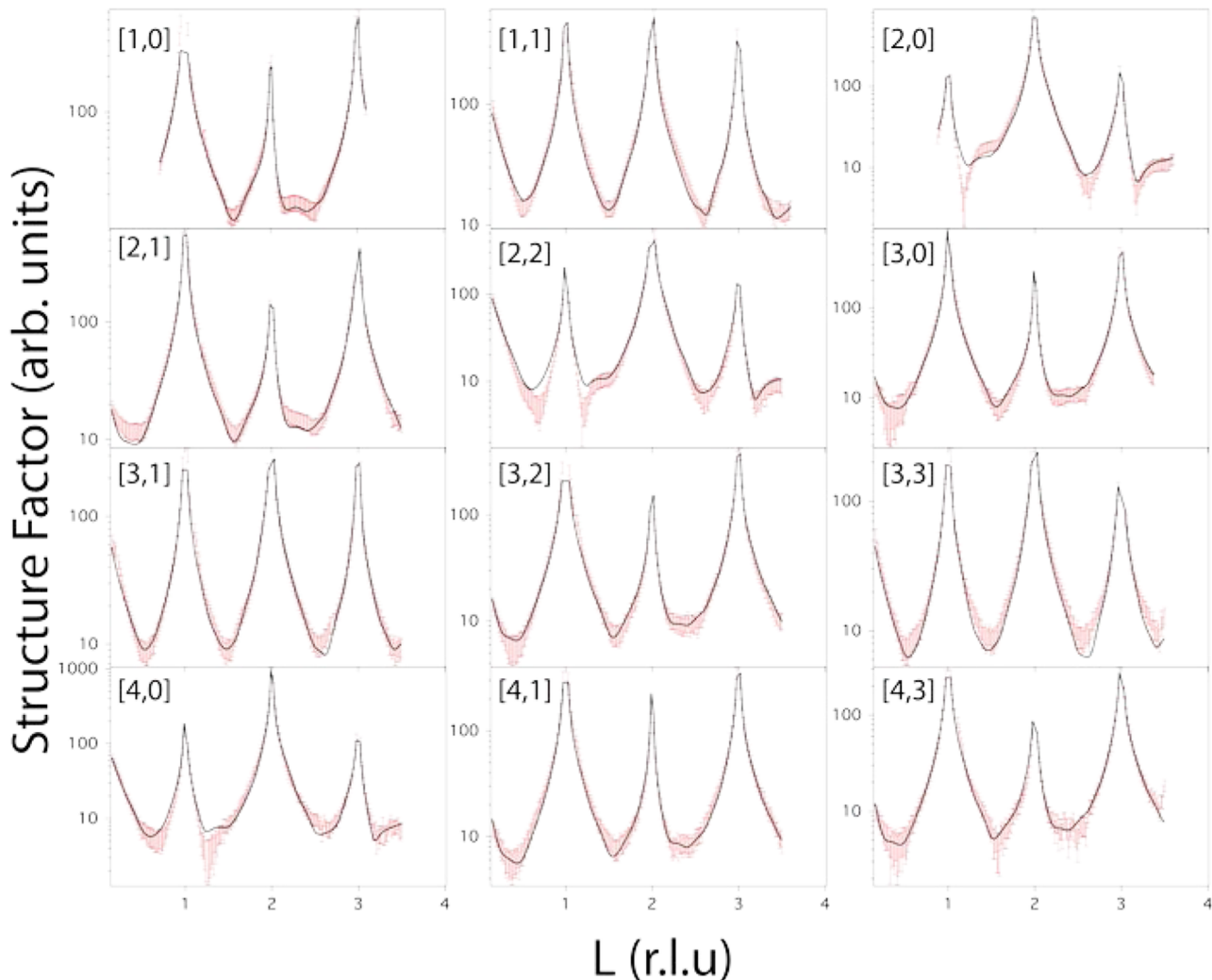


**Figure 3.** Best-fit to the CTRs for the clean  $\text{SrTiO}_3$  (001) surface. Red error bars and solid black line are experimental and calculated structure factors (best-fit), respectively.

black, blue, and red error bars are the clean, water-adsorbed, and nitrogen flow structure factors, respectively. It should be noted that fractional order rods (FORs) were also investigated for each condition, but no intensity was found. From the analysis of the experimental data for each condition, the standard deviations  $\sigma_{h,k,l}$  of the structure factor amplitudes  $|F_{h,k,l}|$  were evaluated by the squared sum of a systematic error, estimated from the measurements of several equivalent reflections to be close to 12%.<sup>23</sup> The analysis of the symmetry-equivalent reflections shows the same  $p4mm$  plane group symmetry for each of the three measured data sets.

## ■ DATA ANALYSIS

The experimental data were tested against model surface structures with a set of free parameters (see below) using a version of the program ROD<sup>22</sup> that utilizes a least-squares refinement procedure. The final goodness-of-fit between experimental data and the calculated structure factors is given in terms of two commonly used parameters  $\chi^2$  (ref 24) and  $R$  (ref 25):

$$\chi^2 = \frac{1}{\sqrt{N-p}} \sum \left( \frac{|F_{h,k,l}^{\text{calc}}|^2 - |F_{h,k,l}^{\text{exp}}|^2}{\sigma_{h,k,l}} \right)^2$$

$$R = \frac{\sum_{h,k,l} ||F_{h,k,l}^{\text{exp}}| - |F_{h,k,l}^{\text{calc}}||}{\sum_{h,k,l} |F_{h,k,l}^{\text{exp}}|}$$

where  $N$  is the number of measured structure factors,  $p$  is the number of independent parameters used in the model,  $F_{h,k,l}^{\text{calc}}$  are the calculated structure factors,  $F_{h,k,l}^{\text{exp}}$  are the experimentally measured structure factors, and  $\sigma_{h,k,l}$  corresponds to the experimental uncertainties.

A  $\chi^2$  value close to 1 indicates a good fit between experiment and theory. The error bars are calculated with a least-squares analysis<sup>24</sup> and correspond to how much a parameter has to be changed while relaxing all others to cause an increase of  $\chi^2$  by a factor of  $1/(N-p)$  from its minimum value.<sup>26</sup> As the  $\chi^2$  is very much dependent on the error bars of the experimental data, one must take care when comparing different values. The parameter  $R$  ( $R$  factor) provides a value that is independent of the error bars and checks the reflection-by-reflection agreement between the observations and the calculations and constitutes another indicator of the reliability of the model. A value close to 10% is considered a small value that would reinforce the reliability of the checked model.<sup>26</sup> The parameters optimized during the fitting procedure were the  $z$ -component of atomic positions, i.e., displacements along the surface normal, overall

isotropic Debye–Waller factors, occupancies of atomic sites, roughness (see, e.g., ref 23) and a scaling factor.

Here we represent water molecules or hydroxyls in the analysis simply as oxygen atoms due to the low X-ray scattering contribution from hydrogen.

## RESULTS AND DISCUSSION

**UHV Surface.** The starting point for the structure determinations was the two possible bulk terminated surfaces

**Table 1. Occupancies of the First Two Atomic Layers for Each Termination of the SrTiO<sub>3</sub>(001) Substrate<sup>a</sup>**

terrace termination	layer	occupancy
T1: TiO <sub>2</sub>	L1 (TiO <sub>2</sub> )	0.29
	L2 (SrO)	0.43
T2: SrO	L3 (SrO)	0.13
	L4 (TiO <sub>2</sub> )	0.64

<sup>a</sup>The layers correspond to Figures 1 and 4. Occupancies apply to all conditions measured in the experiment.

of the STO (001) substrate (i.e., TiO<sub>2</sub> and SrO). Structure factors for both surfaces were computed assuming a single termination with fully occupied atomic positions. However, both produced a poor fit to the experimental data, having a minimum  $\chi^2$  value of 3.3. A reasonable fit to the data could only be achieved with a model consisting of a surface with both types of termination. A total of 77 free fitting parameters were used for the analysis. Allowing displacements, i.e., fitting the z-component of the position of all atoms to a depth of 6 unit cells (12 atomic layers) for the TiO<sub>2</sub>-terminated terrace and 5.5 unit cells for the SrO-terminated terrace, resulted in 60 parameters, i.e., 32 and 28 structural parameters for each of the TiO<sub>2</sub>- and SrO-terminated terraces, respectively. Taking into account disorder in-plane gave 10 (static) Debye–Waller parameters and 5 parameters allowing for partial occupancy of SrO and TiO<sub>2</sub> in the first 2 atomic layers. Finally, we allowed for roughness and introduced a scaling parameter. A  $\chi^2$  value of 1.0 and R-value of 0.12 was produced which indicates the excellent agreement between the experimentally measured and calculated structure factors, visually evidenced in Figure 3.

As noted above, the STO(001) model that gives the best fit to the data is formed by two different types of terraces, with the topmost layer being either TiO<sub>2</sub> or SrO. The intensity contribution to each of the terraces to the reflections measured

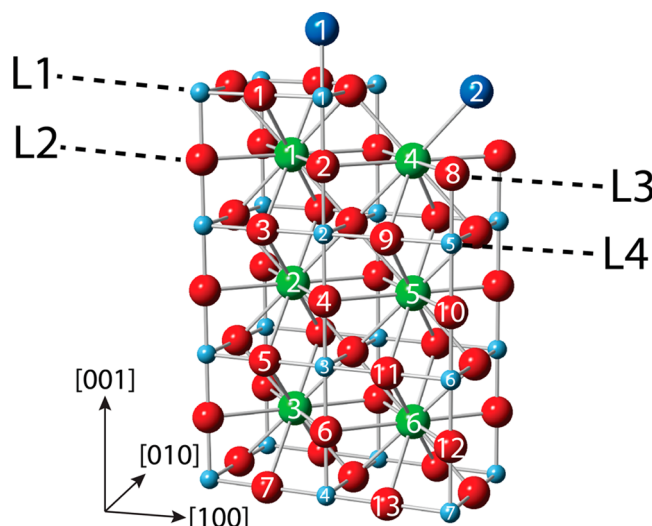


**Figure 4.** Ball-and-stick model representation of SrTiO<sub>3</sub>(001) surface with water adsorption. Color scheme same as Figure 1. Large dark blue spheres are either H<sub>2</sub>O(1) or OH(2). The labeled layers (L1, L2, L3, and L4) are the same as used in Table 1. The numbering of the Ti, Sr, and O atoms is the same as used in Table 2 and 3.

must be added independently (incoherently). When adding the scattering contributions from both terraces coherently, the fit gets much worse producing a best  $\chi^2$  value of only 4.4. Hence, the individual areas of each of these terraces are larger than the coherence length of the X-rays. The topmost layer of terrace 1 (T1) and terrace 2 (T2) will be TiO<sub>2</sub> and SrO, respectively, as shown in Figure 1. Early stages of the refinement of the structural model revealed the necessity of including vacancies in the two topmost surface layers. These surface defects will have been produced by the cleaning procedure. For this reason, the  $\beta$ -model<sup>27</sup> for the parametrization of the surface roughness does not provide a sufficiently precise description. This arises because this model does not allow a variation of the occupancies from layer to layer within the unit cell. For this reason we carried out a refinement of the occupancy (cf. Table 1) of the two topmost STO layers belonging to each terrace (L1–L4 in Figure 1). The missing atoms (vacancies) in the two topmost layers expose the layers below, needs to be taken into account when estimating the final fraction of TiO<sub>2</sub>- and SrO-terminated surface areas. It should be noted that the surface coverage (Cov) of the total of both terraces is 1 (Cov[T1] = 1

**Table 2. Comparison of the Atomic Displacements in the [001] Direction, i.e., along the Surface Normal between the UHV Prepared Mixed Terminated SrTiO<sub>3</sub>(001) Surface from This Work, with Other Reported Values<sup>a</sup>**

termination	atom	this work (68:32)	atomic displacements ( $\text{\AA}$ )			
			SXRD <sup>29</sup> (78:22)	SXRD <sup>30</sup> (66:33)	ref 16	B3LYP
TiO <sub>2</sub>	Ti(1)	$-0.12 \pm 0.02$	$0.00 \pm 0.03$	-0.02	-0.15	-0.11
	O(1)	$-0.23 \pm 0.06$	$-0.5 \pm 0.3$	-0.37	-0.08	-0.03
	Sr(1)	$-0.06 \pm 0.01$	$-0.01 \pm 0.01$	-0.01	0.09	0.14
	O(2)	$0.04 \pm 0.02$	$0.2 \pm 0.1$	0.39	-0.01	0.00
SrO	Sr(4)	$0.10 \pm 0.01$	$-0.25 \pm 0.07$	0.09	-0.12	-0.22
	O(8)	$0.27 \pm 0.05$	$-0.3 \pm 0.4$	0.2 <sup>b</sup>	0.05	0.01
	Ti(5)	$0.09 \pm 0.01$	$-0.24 \pm 0.07$	0.2	0.07	0.06
	O(9)	$-0.08 \pm 0.02$	$-0.4 \pm 0.7$	-0.37	0.06	0.03

<sup>a</sup>The atom labels correspond with those seen in Figure 1. A negative value indicates an atom displacing towards the bulk. Also shown is the TiO<sub>2</sub>/SrO ratio for each experimental study. <sup>b</sup>Indicates very large error up to 50%. Reference 30 has an average error of  $\pm 0.02 \text{ \AA}$ .

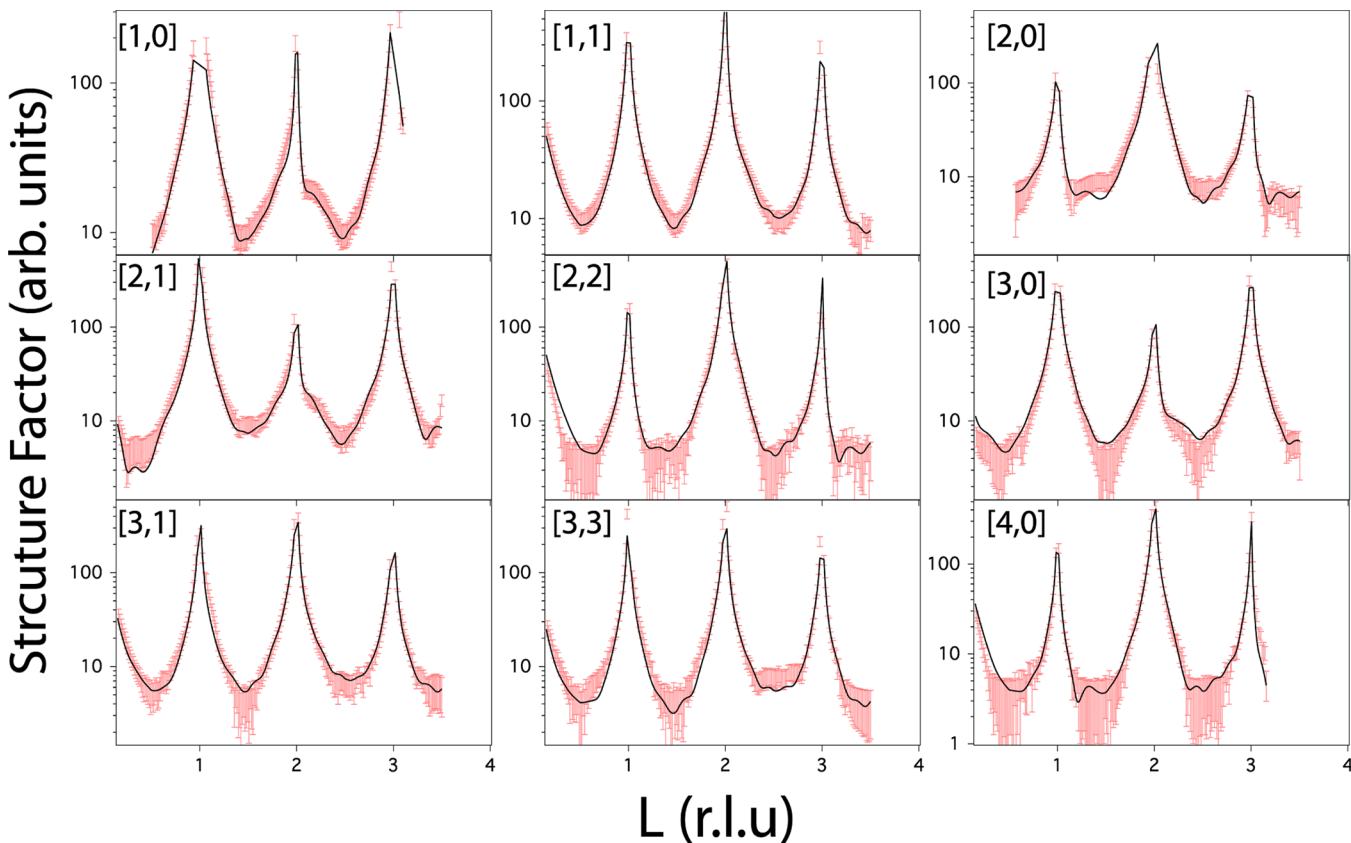


**Figure 5.** CTRs for the water-adsorbed  $\text{SrTiO}_3(001)$  surface. Red error bars and solid black line are the experimentally measured and calculated structure factors (best-fit), respectively.

$- \text{Cov}[\text{T}2])$  while the refinement of the occupancy layers L1, L2 belonging to (T1) and L3 and L4 belonging to (T2) gives a  $\text{TiO}_2/\text{SrO}$  surface distribution involving four layers. The  $\text{TiO}_2/\text{SrO}$  surface coverage is 68:32% (cf. Table 1),<sup>28</sup> with a roughness parameter of  $\beta = 0.2$ .

If the roughness parameter is refined only, i.e., the occupancies of the atoms in both terraces are fixed to 1, then the roughness parameter increases to  $\beta = 0.4$ . This result is consistent with the model above as it also describes, though in a more global way, partially occupied atomic positions in the two topmost surface layers. According to the  $\beta$  roughness model,<sup>27</sup> with a value of  $\beta = 0.4$  the topmost and second surface layer would have an occupancy of 0.16 and 0.4, respectively, and the third layer would be fully occupied. These values are very close to those listed in Table 1. The atomic displacements of the first two atomic layers from both terminations of the best-fit model of this study and that of others in the literature<sup>16,29,30</sup> are given in Table 2, with the atom labels corresponding with those used in Figure 1.

It has been suggested by Ravikumar et al.<sup>31</sup> that lateral displacements are present in the SrO termination of the substrate thus breaking the fourfold symmetry. However, the fact that LEED produced a clear  $(1 \times 1)$  pattern and no fractional order rods were found suggests that the surface was not reconstructed under our preparation conditions. Consequently, the cations were only permitted to move along the  $[001]$  direction. This maintains the  $p4mm$  symmetry of the surface.

When comparing our findings with other results reported in the literature, it is quite clear from Table 2 that the atomic displacements given in ref 30 agree best with our study overall,

where the atomic shift directions from the two topmost layers of both terraces, T1 and T2, are identical. Moreover, this agreement is especially highlighted for Sr(4) of the SrO-terminated terrace which in the earlier work is found to displace away from the bulk by  $0.09 \pm 0.02 \text{ \AA}$  similar to the displacement of  $0.10 \pm 0.01 \text{ \AA}$  found here. In contrast, the two other studies<sup>16,29</sup> find a strong negative displacement, i.e., toward the bulk. Except for Ti(5), the displacements of the cations given in ref 30 are slightly smaller. However, the general trend is similar to our results. Similarly, for the  $\text{TiO}_2$ -terminated terrace the atomic positions given in ref 30 match better with our values than those from the other two publications. For both terminated terraces, the cations displace in the same direction with a similar magnitude as found here, i.e., inward for the  $\text{TiO}_2$ -terminated terrace and outward for the SrO termination. As regards the anions, the results presented here and in ref 30 show that O(1) exhibits a much larger displacement whereas O(2) displaces much less in our case. For each terrace, both types of oxygen atoms relax in opposing directions: inward for O(1) and outward for O(2); outward for O(8) and inward for O(9). In this respect also, only the results published in ref 30 are in reasonable agreement with our findings.

The lack of agreement with the results from ref 29 for the atomic positions of the  $\text{TiO}_2$ -terminated terrace is notable. However, our results are in striking disagreement regarding the SrO-terminated terrace. This is especially the case for Sr(4) of the SrO-terminated surface, which displaces in the opposite direction. Similarly pronounced is the disagreement for the other atomic positions of the SrO-terminated terrace. Large inward displacements are reported for all atoms of the SrO terrace in ref 29 whereas we find that Sr(4), Ti(5), and O(8) all

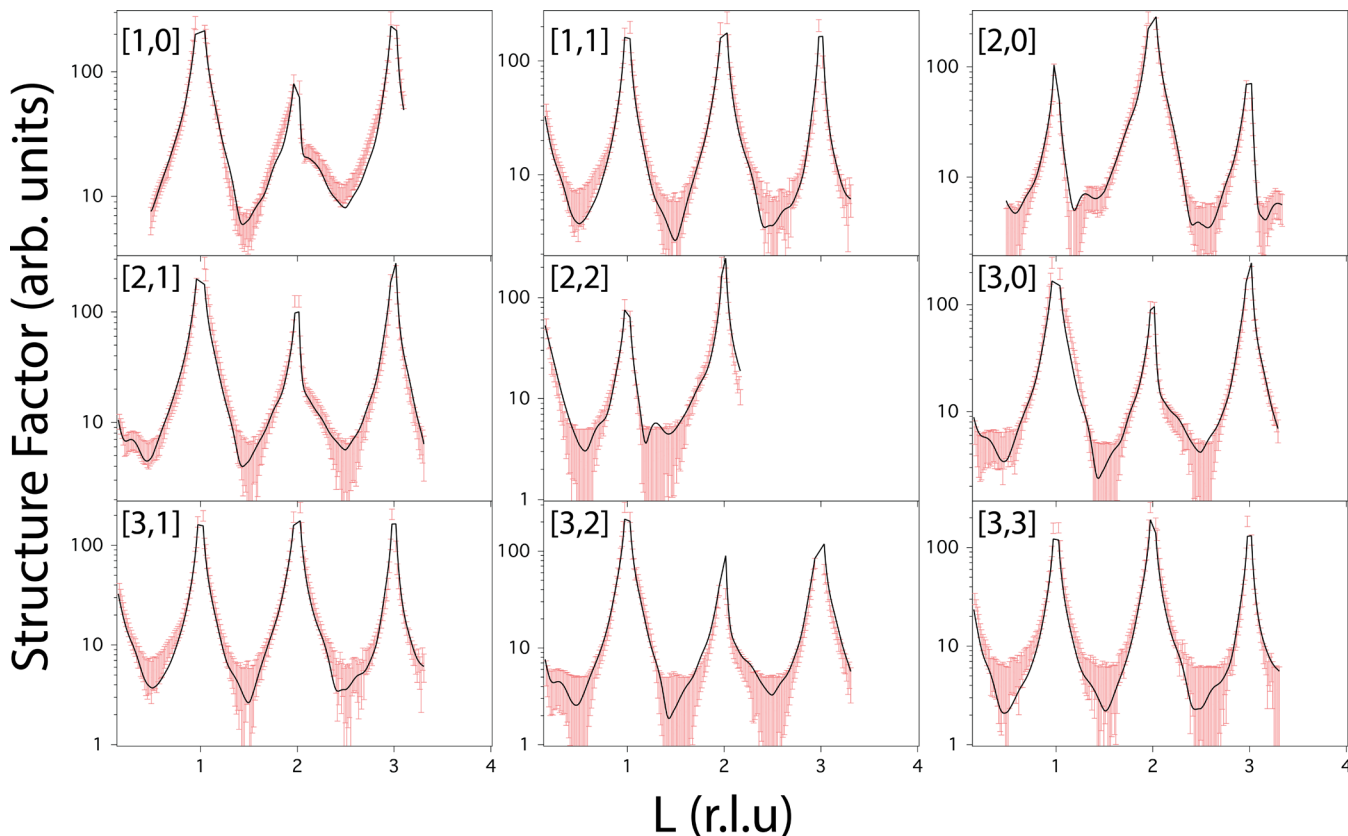


**Figure 6.** CTRs for the nitrogen blow-dried  $\text{SrTiO}_3$  (001) surface. Red error bars and solid black line are experimental and calculated structure factors (best-fit), respectively.

displace outward by  $0.10 \pm 0.01$ ,  $0.09 \pm 0.01$ , and  $0.27 \pm 0.05$  Å, respectively. We find only for O(9) an inward-displacement, but with a much smaller magnitude than listed in ref 29.

Neither of the two calculations from the theoretical study by Evestrov et al., ref 16, shows reasonable agreement with the present or any of the other two experimental studies, except for Ti(1) in the  $\text{TiO}_2$ -terminated terrace. Large differences in the relaxation are seen with all other atoms in this termination, particularly for Sr(1) and O(2). Similarly, discrepancies are seen for the SrO-terminated terrace, with Sr(4) and O(9) shown to displace in directions opposite to those found here.

A possible origin of the reasonable agreement between the results of the present study and ref 30 and poor agreement with ref 29 may be the preparation method, which strongly influences the  $\text{TiO}_2/\text{SrO}$  termination ratio and structure of the surface.<sup>32,33</sup> In ref 30 the authors studied several samples prepared in different ways. The displacements shown in Table 2 were found for a sample that was given a final annealing in 0.1 mbar  $\text{O}_2$  at 700 °C after etching and annealing in a tube furnace. For this sample it was reported that it had a ratio of 66:33 of  $\text{TiO}_2/\text{SrO}$ -terminated surface areas. Although it showed a (2 × 2) reconstruction, the  $\text{TiO}_2/\text{SrO}$  ratio is closer to the ratio (68/32) for the sample of this study whereas the sample of ref 29, prepared by sputter/annealing (900 K) cycles, had a ratio of 78:22  $\text{TiO}_2/\text{SrO}$ .

An important question to answer is whether the perfect, ideal termination of the STO(001) ( $1 \times 1$ ) surface exists. Early experimental work, such as a combined LEED and AR-XPS investigation<sup>34</sup> on the Ti-rich surface, suggests that it does not. They found that the unreconstructed p( $1 \times 1$ ) STO(001) surface, terminated with a  $\text{TiO}_2$  layer and obtained by simple

chemical etching, is always accompanied by the presence of oxygen vacancies. These findings are in agreement with several X-ray and electron scattering experiments<sup>35–37</sup> that detect the presence of oxygen vacancies and surface buckling. It is surprising, given the stability of the ( $1 \times 1$ ) surface, that there is a scarcity of atomically resolved images displaying the coexistence of  $\text{TiO}_2/\text{SrO}$  terraces (step height ~ 2 Å). However, using *in situ* fracturing of STO at room temperature, Guisinger et al.<sup>38</sup> observed the coexistence of  $\text{TiO}_2/\text{SrO}$  terraces by STM. With regard to the electronic structure, according to the formal valences of  $\text{Ti}^{4+}$ ,  $\text{Sr}^{2+}$ , and  $\text{O}^{2-}$ , the STO(001) surface would not be polar. However, the real valences are considerably different,<sup>39,40</sup> resulting in an excess of negative and positive charge on the  $\text{TiO}_2$  and SrO planes, respectively. The electrostatic charge of the order of  $\pm 0.5 \text{ e}_0$  renders the (001) axis (weakly) polar, contrary to simple expectations. As a consequence, the ideal SrO- or  $\text{TiO}_2$ -terminated surfaces of  $\text{SrTiO}_3(001)$  cannot be stable and must relax or reconstruct as shown by the calculations and experimental work. Surface roughness and/or changes in the stoichiometry, as observed in the present study, will also contribute to a lowering of the electrostatic energy. However, these modifications, which will also depend on specific preparation procedures, would be very difficult to take into account by total energy calculations.

**STO(001) in Contact with Water.** As mentioned above, quantitative experimental investigations of the STO(001)/ $\text{H}_2\text{O}$  interface are quite scarce. On the other hand, several theoretical investigations<sup>4,6,15–17</sup> have been conducted. The general consensus seems to be that water adsorption is more reactive on the SrO-terminated surface, leading to molecular and

**Table 3. Experimentally Determined Atomic Displacements in the [001] Direction, i.e., Normal to the Surface, for the UHV-Prepared, Water-Adsorbed, and Nitrogen-Dried  $\text{SrTiO}_3$  (001) Surface<sup>a</sup>**

atom	atomic displacements ( $\text{\AA}$ )		
	clean (UHV)	water	$\text{N}_2$
Ti(1)	-0.12 $\pm$ 0.02	-0.12 $\pm$ 0.03	-0.23 $\pm$ 0.05
O(1)	-0.23 $\pm$ 0.06	-0.16 $\pm$ 0.07	0.08 $\pm$ 0.13
Sr(1)	-0.06 $\pm$ 0.01	0.09 $\pm$ 0.01	0.15 $\pm$ 0.01
O(2)	0.04 $\pm$ 0.02	0.04 $\pm$ 0.06	0.09 $\pm$ 0.09
Ti(2)	-0.16 $\pm$ 0.01	0.19 $\pm$ 0.01	0.13 $\pm$ 0.01
O(3)	-0.03 $\pm$ 0.01	-0.23 $\pm$ 0.02	-0.10 $\pm$ 0.03
Sr(2)	-0.11 $\pm$ 0.01	0.04 $\pm$ 0.01	0.02 $\pm$ 0.01
O(4)	-0.02 $\pm$ 0.02	0.23 $\pm$ 0.02	0.23 $\pm$ 0.04
Ti(3)	-0.15 $\pm$ 0.01	0.06 $\pm$ 0.01	-0.01 $\pm$ 0.01
O(5)	0.05 $\pm$ 0.01	0.02 $\pm$ 0.08	0.01 $\pm$ 0.03
Sr(3)	-0.01 $\pm$ 0.01	0.09 $\pm$ 0.01	0.03 $\pm$ 0.01
O(6)	-0.22 $\pm$ 0.01	-0.18 $\pm$ 0.02	-0.19 $\pm$ 0.03
Ti(4)	-0.04 $\pm$ 0.01	0.01 $\pm$ 0.01	-0.05 $\pm$ 0.01
O(7)	-0.19 $\pm$ 0.01	0.12 $\pm$ 0.08	-0.08 $\pm$ 0.02
Sr(4)	<b>0.10 <math>\pm</math> 0.01</b>	<b>0.23 <math>\pm</math> 0.04</b>	<b>0.19 <math>\pm</math> 0.04</b>
O(8)	<b>0.27 <math>\pm</math> 0.05</b>	<b>0.03 <math>\pm</math> 0.21</b>	<b>0.06 <math>\pm</math> 0.37</b>
Ti(5)	<b>0.09 <math>\pm</math> 0.01</b>	<b>-0.12 <math>\pm</math> 0.01</b>	<b>0.01 <math>\pm</math> 0.01</b>
O(9)	-0.08 $\pm$ 0.02	0.23 $\pm$ 0.02	0.23 $\pm$ 0.03
Sr(5)	<b>0.10 <math>\pm</math> 0.01</b>	<b>0.06 <math>\pm</math> 0.01</b>	<b>0.07 <math>\pm</math> 0.01</b>
O(10)	<b>-0.23 <math>\pm</math> 0.01</b>	<b>-0.23 <math>\pm</math> 0.02</b>	<b>-0.23 <math>\pm</math> 0.03</b>
Ti(6)	<b>0.14 <math>\pm</math> 0.01</b>	<b>-0.02 <math>\pm</math> 0.01</b>	<b>-0.03 <math>\pm</math> 0.01</b>
O(11)	<b>0.11 <math>\pm</math> 0.01</b>	<b>-0.11 <math>\pm</math> 0.02</b>	<b>-0.03 <math>\pm</math> 0.01</b>
Sr(6)	<b>0.09 <math>\pm</math> 0.01</b>	<b>0.01 <math>\pm</math> 0.01</b>	<b>0.05 <math>\pm</math> 0.01</b>
O(12)	<b>0.20 <math>\pm</math> 0.01</b>	<b>0.23 <math>\pm</math> 0.08</b>	<b>0.08 <math>\pm</math> 0.02</b>
Ti(7)	<b>0.09 <math>\pm</math> 0.01</b>	<b>0.01 <math>\pm</math> 0.01</b>	<b>0.03 <math>\pm</math> 0.01</b>
O(13)	<b>0.01 <math>\pm</math> 0.01</b>	<b>0.19 <math>\pm</math> 0.02</b>	<b>-0.04 <math>\pm</math> 0.02</b>

<sup>a</sup>The atom labels correspond with those seen in Figure 1 and 5. Highlighted in bold are the atoms associated with the SrO-terminated terrace. A negative value indicates an atom displacing towards the bulk.

dissociative adsorption. In contrast, only molecular adsorption occurs on the  $\text{TiO}_2$  termination. Following from the structure determined for the clean surface, we started the analysis by positioning  $\text{H}_2\text{O}/\text{OH}$  molecules on both terminations. There was no change in the  $\text{TiO}_2/\text{SrO}$  ratio (i.e., both the surface percentage of each termination type (50%) and the occupancies of the  $\text{TiO}_2$  and SrO terraces in the two topmost surface layers were exactly the same as for the clean surface (Table 1)). This indicates that water adsorption has little effect on the stoichiometry of the substrate. The roughness parameter for the water-covered surface increased to 0.4 from 0.2 for the clean surface. Oxygen atoms of the  $\text{H}_2\text{O}/\text{OH}$  molecules were allowed the freedom to displace in-plane, in both the [010] and [100] directions. The most favored adsorption site found for the  $\text{TiO}_2$ -terminated terrace is atop titanium. For the SrO-terminated terrace, the favored position is the same as that which an oxygen atom would occupy if the perovskite lattice were extended into the vacuum. This agrees well with the literature.<sup>16,17,41</sup> The best-fit model is shown in Figure 4 and produced a  $\chi^2$  value of 1.4 and  $R$ -value of 0.16. This indicates a very good agreement between experiment and the best fit model, as visually evidenced in Figure 5.

The X-ray scattering strength is proportional to the electron density, and thus it is extremely difficult in a surface X-ray diffraction experiment to distinguish between  $\text{H}_2\text{O}$ , OH, and O on the STO surface because of the low scattering contribution

from hydrogen. However, in order to deduce whether an oxygen atom is in its atomic form, protonated or doubly protonated, bond distances can provide indirect evidence. Starting first with the  $\text{TiO}_2$ -terminated terrace, the distance between the oxygen of the (presumed)  $\text{H}_2\text{O}(1)$  and Ti(1) was found to be  $2.30 \pm 0.04 \text{ \AA}$ , which is in good agreement with the literature bond distances of 2.21,<sup>41</sup> 2.26,<sup>16</sup> and 2.27  $\text{\AA}$ <sup>17</sup> for molecular water adsorption on the STO surface. This is strong evidence that the mode of adsorption favored for the  $\text{TiO}_2$ -terminated terrace is molecular in nature. For the SrO-terminated terrace, the distance between Sr(4) and the oxygen in OH(2) was found to be  $2.60 \pm 0.04 \text{ \AA}$ , again in excellent agreement with the literature values of 2.59,<sup>41</sup> 2.61,<sup>16</sup> and 2.55  $\text{\AA}$ <sup>17</sup> for dissociative adsorption on the STO surface. The occupancies of  $\text{H}_2\text{O}(1)$  and OH(1) sites were found to be  $0.89 \pm 0.07$  and  $0.79 \pm 0.06$ , respectively. Furthermore, in the literature it is suggested that with the dissociation of the water molecule, the liberated hydrogen atom forms a H-bond with the surface oxygen atom, i.e., O(8) of the substrate creating a second OH. In our case this determination is very difficult because of the insensitivity of this atom to out-of-plane displacements and its large associated error. This is mainly due to both the low atomic number of the oxygen atom O(8) and its low site occupancy, as indicated in Table 1. Nevertheless, the excellent agreement of the bond distances of Sr(4) and OH(2) leads us to believe dissociation is the favored adsorption mode.

**Nitrogen.** After the measurements were completed for the water-adsorbed surface, a flow of nitrogen was used to evaporate the water droplet. Since the atmosphere within the chamber after this process is saturated with water, it was expected that the surface would be very similar to the water-covered surface and was thus used as the starting point for analysis. The best-fit produced a  $\chi^2$  value of 1.5 and  $R$ -value of 0.19, and the comparison between the experimental data and best-fit are shown in Figure 6. Again, no change was detected in the surface percentage of each termination type (50%), and the occupancies of the  $\text{TiO}_2$  and SrO terraces in the two topmost surface layers were exactly the same as for the other two surfaces studied. The roughness parameter was 0.4, the same as for the STO(001)-liquid water interface. All of this points to the stoichiometry being insensitive to water adsorption. By inspection of Figure 2 and Table 3, it is obvious that the atomic displacements of the  $\text{N}_2$ -dried surface are very similar to those for the water-covered surface rather than those of the clean surface. This is especially the case for the surface cations (Ti(1) and Sr(1)) of the  $\text{TiO}_2$ -terminated terrace, which are displaced in similar directions and magnitudes. The largest difference between the  $\text{N}_2$ -dried and the water-covered surface is that the sites  $\text{H}_2\text{O}(1)$  and OH(1), i.e., the oxygen atoms representing the  $\text{H}_2\text{O}/\text{OH}$  molecule, were found to have an occupancy of 0 by the fit. Furthermore, larger displacements and error bars are seen for the O(7) and for the cations (Ti(3) and Ti(4)), which now are displaced in opposite directions. As for the SrO-terminated terrace, the cations and anions largely show similar displacements to the water-covered surface, with the exceptions being Ti(5) and O(13) displacing in opposite directions. The close similarity of atomic displacements between this condition and the water-covered condition lead us to believe that most likely a highly disordered overlayer of water is present on the surface.

## SUMMARY

SXRD results demonstrate that the  $\text{SrTiO}_3(001)$  surface, prepared by annealing in  $1 \times 10^{-2}$  mbar  $\text{O}_2$  partial pressure, is comprised of terraces that exhibit either a  $\text{SrO}$  or  $\text{TiO}_2$  terminating layer. They cover equally large areas, and the resulting scattering signal is an incoherent superposition of the signals originating from both terraces. The first two layers of both terraces are only partially occupied, and this leads to a final surface coverage  $\text{TiO}_2:\text{SrO}$  ratio of 68:32. When contacting this surface under controlled conditions with a drop of water, our results suggest that the adsorption mode favored for the  $\text{TiO}_2$ -terminated terrace is molecular in nature with the bonding position atop Ti. On the other hand, for the  $\text{SrO}$ -terminated terrace it appears that dissociation is the adsorption mode, with the oxygen atom of the OH positioned where an oxygen would be located if the perovskite lattice was extended. Removal of the water droplet with a flow of nitrogen led to a surface structure that is similar to the water-covered surface, although probably with a disordered overlayer of water. This is reflected in the similarity of atomic displacements between the water-covered surface and nitrogen-dried surface. The ratio of the  $\text{TiO}_2$  and  $\text{SrO}$  covered surface areas and the layer occupancies did not change over the course of the experiment, indicating that water does not influence the cation concentration at the  $\text{STO}(001)$  surface.

## AUTHOR INFORMATION

### Corresponding Author

\* Tel.: +442076797979; e-mail: g.thornton@ucl.ac.uk.

### Present Addresses

<sup>†</sup>The University of Manchester, School of Materials, Photon Science Institute, Alan Turing Building, Oxford Road, Manchester M13 9PL, U.K.

<sup>‡</sup>Bhaba Atomic Research Centre, Atomic and Molecular Physics Division, Trombay, Mumbai-85, India, Mumbai, IN 400-085.

<sup>§</sup>Dipartimento di Ingegneria Civile, Ambientale e dei Materiali, Università di Bologna, Via Terracini 28, 40131 Bologna, Italy.

<sup>△</sup>Diamond Light Source Ltd., Diamond House, Harwell Science and Innovation Campus, Didcot, Oxfordshire OX11 0DE, U.K.

### Notes

The authors declare no competing financial interest.

## ACKNOWLEDGMENTS

We thank Martin Castell for useful discussions. Skillful technical assistance of Helena Isern and Lionel André at the ID32 beamline is gratefully acknowledged. This work was funded by grants from the EPSRC (U.K.) (EP/CS41898/1), M.E.C. (Spain) through projects CSD2007-00041 and MAT2012-38213-C02-02, EU ITN SMALL, COST Action CM1104, ERC Advanced Grant ENERGYSURF (GT), and the Royal Society.

## REFERENCES

- (1) Wagner, F.; Ferrer, S.; Somorjai, G. Photocatalytic Hydrogen Production from Water over  $\text{SrTiO}_3$  Crystal Surfaces, Electron Spectroscopy Studies of Adsorbed  $\text{H}_2$ ,  $\text{O}_2$ , and  $\text{H}_2\text{O}$ . *Surf. Sci.* **1980**, *101*, 462–474.
- (2) Hodak, S. K.; Supasai, T.; Wisitsoraat, A.; Hodak, J. H. Design of Low Cost Gas Sensor Based on  $\text{SrTiO}_3$  and  $\text{BaTiO}_3$  Films. *J. Nanosci. Nanotechnol.* **2010**, *10*, 7236–7238.
- (3) Blennow, P.; Hagen, A.; Hansen, K. K.; Wallenberg, L. R.; Mogensen, M. Defect and Electrical Transport Properties of Nb-Doped  $\text{SrTiO}_3$ . *Solid State Ion.* **2008**, *179*, 2047–2058.
- (4) Shi, W.-J.; Xiong, S.-J. Ab Initio Study of Water Adsorption on  $\text{TiO}_2$  Terminated (100) Surface of  $\text{SrTiO}_3$  with and without Cr Doping. *Surf. Sci.* **2010**, *604*, 1987–1995.
- (5) Wang, L.-Q.; Ferris, K. F.; Herman, G. S. Interactions of  $\text{H}_2\text{O}$  with  $\text{SrTiO}_3(100)$  Surfaces. *J. Vac. Sci. Technol., A* **2002**, *20*, 239–244.
- (6) Wei, W.; Dai, Y.; Guo, M.; Ma, Y.; Huang, B. Atomic Pt and Molecular  $\text{H}_2\text{O}$  Adsorptions on  $\text{SrTiO}_3$  with and without Nb-Doping: Electron Trapping Center and Mediating Roles of Pt in Charge Transfer from Semiconductor to Water. *J. Solid State Chem.* **2012**, *187*, 64–69.
- (7) Lin, Y.; Becerra-Toledo, A. E.; Silly, F.; Poeppelmeier, K. R.; Castell, M. R.; Marks, L. D. The  $(2 \times 2)$  Reconstructions on the  $\text{SrTiO}_3(001)$  Surface: A Combined Scanning Tunneling Microscopy and Density Functional Theory Study. *Surf. Sci.* **2011**, *605*, L51–L55.
- (8) Becerra-Toledo, A. E.; Castell, M. R.; Marks, L. D. Water Adsorption on  $\text{SrTiO}_3(001)$ : I. Experimental and Simulated STM. *Surf. Sci.* **2012**, *606*, 762–765.
- (9) Becerra-Toledo, A. E.; Enterkin, J. A.; Kienzle, D. M.; Marks, L. D. Water Adsorption on  $\text{SrTiO}_3(001)$ : II. Water, Water, Everywhere. *Surf. Sci.* **2012**, *606*, 791–802.
- (10) Marshall, M. S. J.; Becerra-Toledo, A. E.; Payne, D. J.; Egddell, R. G.; Marks, L. D.; Castell, M. R. Structure and Composition of Linear  $\text{TiO}_x$  Nanostructures on  $\text{SrTiO}_3(001)$ . *Phys. Rev. B* **2012**, *86*, 125416–125416–6.
- (11) Erdman, N.; Warschkow, O.; Asta, M.; Poeppelmeier, K. R.; Ellis, D. E.; Marks, L. D. Surface Structures of  $\text{SrTiO}_3(001)$ : A  $\text{TiO}_2$ -Rich Reconstruction with a  $c(4 \times 2)$  Unit Cell. *J. Am. Chem. Soc.* **2003**, *125*, 10050–10056.
- (12) Erdman, N.; Marks, L. D.  $\text{SrTiO}_3(001)$  Surface Structures under Oxidizing Conditions. *Surf. Sci.* **2003**, *526*, 107–114.
- (13) Newell, D. T.; Harrison, A.; Silly, F.; Castell, M. R.  $\text{SrTiO}_3(001)-(\sqrt{5} \times \sqrt{5})-\text{R}26.6^\circ$  Reconstruction: A Surface Resulting from Phase Separation in a Reducing Environment. *Phys. Rev. B* **2007**, *75*, 205429–205429–9.
- (14) Iwahori, K.; Watanabe, S.; Kawai, M.; Kobayashi, K.; Yamada, H.; Matsushige, K. Effect of Water Adsorption on Microscopic Friction Force on  $\text{SrTiO}_3(001)$ . *J. Appl. Phys.* **2003**, *93*, 3223–3227.
- (15) Baniecki, J. D.; Ishii, M.; Kurihara, K.; Yamanaka, K.; Yano, T.; Shinozaki, K.; Imada, T.; Kobayashi, Y. Chemisorption of Water and Carbon Dioxide on Nanostructured  $\text{BaTiO}_3-\text{SrTiO}_3(001)$  Surfaces. *J. Appl. Phys.* **2009**, *106*, 054109–054109–12.
- (16) Evarestov, R. A.; Bandura, A. V.; Alexandrov, V. E. Adsorption of Water on (001) Surface of  $\text{SrTiO}_3$  and  $\text{SrZrO}_3$  Cubic Perovskites: Hybrid HF-DFT LCAO Calculations. *Surf. Sci.* **2007**, *601*, 1844–1856.
- (17) Hinojosa, B. B.; Van Cleve, T.; Asthagiri, A. A First-Principles Study of  $\text{H}_2\text{O}$  Adsorption and Dissociation on the  $\text{SrTiO}_3(100)$  Surface. *Mol. Simul.* **2010**, *36*, 604–617.
- (18) Zegenhagen, J.; Detlefs, B.; Lee, T.-L.; Thiess, S.; Isern, H.; Petit, L.; André, L.; Roy, J.; Mi, Y.; Joumard, I. X-Ray Standing Waves and Hard X-Ray Photoelectron Spectroscopy at the Insertion Device Beamline ID32. *J. Electron Spectrosc. Relat. Phenom.* **2010**, *178*–179, 258–267.
- (19) Jiang, Q. D.; Zegenhagen, J.  $c(6 \times 2)$  and  $c(4 \times 2)$  Reconstruction of  $\text{SrTiO}_3(001)$ . *Surf. Sci.* **1999**, *425*, 343–354.
- (20) Kato, H. S.; Shiraki, S.; Nantoh, M.; Kawai, M. Water Reaction on  $\text{SrTiO}_3(001)$ : Promotion Effect Due to Condensation. *Surf. Sci.* **2003**, *544*, L722–L728.
- (21) Renner, F. U.; Gründer, Y.; Zegenhagen, J. Portable Chamber for the Study of UHV Prepared Electrochemical Interfaces by Hard X-ray Diffraction. *Rev. Sci. Instrum.* **2007**, *78*, 033903–033903–8.
- (22) Vlieg, E. ROD: A Program for Surface X-Ray Crystallography. *J. Appl. Crystallogr.* **2000**, *33*, 401–405.
- (23) Robinson, I. K. *Handbook of Synchrotron Radiation*; North Holland: Amsterdam, 1991; Vol. 3.
- (24) Feidenhans'l, R. Surface Structure Determination by X-ray Diffraction. *Surf. Sci. Rep.* **1989**, *10*, 105–188.

- (25) Stout, G. H.; Jensen, L. H. *X-ray Structure Determination*; McMillan: New York, 1968.
- (26) Lohmeier, M.; Vlieg, E. Angle Calculations for a Six-Circle Surface X-Ray Diffractometer. *J. Appl. Crystallogr.* **1993**, *26*, 706–716.
- (27) Robinson, I. K. Crystal Truncation Rods and Surface Roughness. *Phys. Rev. B* **1986**, *33*, 3830–3836.
- (28) In the case where  $\text{Cov}[\text{T1}] = \text{Cov}[\text{T2}] = 0.5$  (= 50%), as found here, the total  $\text{TiO}_2$  and  $\text{SrO}$  surface coverage obtained from both terminations would be given by  $\text{Cov}(\text{TiO}_2) = \text{Cov}(\text{TiO}_2:\text{T1}) + \text{Cov}(\text{TiO}_2:\text{T2}) = [\text{occ}(\text{L1}) + (1 - \text{occ}(\text{L2})) + [\text{occ}(\text{L4}) - \text{occ}(\text{L3})]$   $\text{Cov}(\text{SrO}) = \text{Cov}(\text{SrO}:\text{T1}) + \text{Cov}(\text{SrO}:\text{T2}) = [\text{occ}(\text{L2}) - \text{occ}(\text{L1})] + [\text{occ}(\text{L3}) + (1 - \text{occ}(\text{L4}))]$ , where the condition  $\text{Cov}(\text{TiO}_2) + \text{Cov}(\text{SrO}) = 1$  holds and  $\text{occ}(\text{Li})$  accounts for the occupancy of layer  $i$  (1–4) from Table 1.
- (29) Charlton, G.; Brennan, S.; Muryn, C. A.; McGrath, R.; Norman, D.; Turner, T. S.; Thornton, G. Surface Relaxation of  $\text{SrTiO}_3(001)$ . *Surf. Sci.* **2000**, *457*, L376–L380.
- (30) Fragneto, A.; De Luca, G. M.; Di Capua, R.; Scotti di Uccio, U.; Salluzzo, M.; Torrelles, X.; Lee, T.-L.; Zegenhagen, J. Ti- and Sr-Rich Surfaces of  $\text{SrTiO}_3$  Studied by Grazing Incidence X-Ray Diffraction. *Appl. Phys. Lett.* **2007**, *91*, 101910–101910–3.
- (31) Ravikumar, V.; Wolf, D.; Dravid, V. Ferroelectric Monolayer Reconstruction of the  $\text{SrTiO}_3(100)$  Surface. *Phys. Rev. Lett.* **1995**, *74*, 960–963.
- (32) Jiang, Q. D.; Zegenhagen, J.  $\text{SrTiO}_3(001)$  Surfaces and Growth of Ultra-Thin  $\text{GdBa}_2\text{Cu}_3\text{O}_{7-\alpha}$  Films Studied by LEED/AES and UHV-STM. *Surf. Sci.* **1995**, *338*, L882–L888.
- (33) Martin R, C. Nanostructures on the  $\text{SrTiO}_3(001)$  Surface Studied by STM. *Surf. Sci.* **2002**, *516*, 33–42.
- (34) <http://meetings.aps.org/link/BAPS.2012.MAR.V18.10>.
- (35) Erdman, N.; Poeppelmeier, K. R.; Asta, M.; Warschkow, O.; Ellis, D. E.; Marks, L. D. The Structure and Chemistry of the  $\text{TiO}_2$ -Rich Surface of  $\text{SrTiO}_3(001)$ . *Nature* **2002**, *419*, 55–58.
- (36) Herger, R.; Willmott, P. R.; Bunk, O.; Schlepütz, C. M.; Patterson, B. D.; Delley, B. Surface of Strontium Titanate. *Phys. Rev. Lett.* **2007**, *98*, 076102–076102–4.
- (37) Becerra-Toledo, A. E.; Marshall, M. S. J.; Castell, M. R.; Marks, L. D. c(4 × 2) and Related Structural Units on the  $\text{SrTiO}_3(001)$  Surface: Scanning Tunneling Microscopy, Density Functional Theory, and Atomic Structure. *J. Chem. Phys.* **2012**, *136*, 214701–214701–9.
- (38) Guisinger, N. P.; Santos, T. S.; Guest, J. R.; Chien, T.-Y.; Bhattacharya, A.; Freeland, J. W.; Bode, M. Nanometer-Scale Striped Surface Terminations on Fractured  $\text{SrTiO}_3$  Surfaces. *ACS Nano* **2009**, *3*, 4132–4136.
- (39) Goniakowski, J.; Noguera, C. The Concept of Weak Polarity: An Application to the  $\text{SrTiO}_3(001)$  Surface. *Surf. Sci.* **1996**, *365*, L657–L662.
- (40) Eglitis, R. I.; Vanderbilt, D. First-Principles Calculations of Atomic and Electronic Structure of  $\text{SrTiO}_3(001)$  and (011) Surfaces. *Phys. Rev. B* **2008**, *77*, 195408–195408–10.
- (41) Guhl, H.; Miller, W.; Reuter, K. Water Adsorption and Dissociation on  $\text{SrTiO}_3(001)$  Revisited: A Density Functional Theory Study. *Phys. Rev. B* **2010**, *81*, 155455–155455–8.